BULLETIN OF THE POLISH ACADEMY OF SCIENCES
TECHNICAL SCIENCES
Vol. 53, No. 3, 2005

# A nonlinear analysis of the human vertebral column and medical recommendations that follow

M. DIETRICH[1]*, K. KĘDZIOR[1], P. BORKOWSKI[1], G. KRZESIŃSKI[1], K. SKALSKI[2], and T. ZAGRAJEK[1]

[1]Institute of Aeronautics and Applied Mechanics, Faculty of Power and Aeronautical Engineering, Warsaw University of Technology, 24 Nowowiejska Str., 00-665 Warsaw, Poland
[2]Faculty of Production Engineering, Warsaw University of Technology, 85 Narbutta Str., 02-524 Warsaw, Poland

**Abstract.** The analysis of mechanical behaviour of spinal column is until now still a challenge, in spite of the great amount of research which has been conducted over the last years. It is a particularly complex structure considering number of components, their shapes and mechanical characteristics. The objectives of the presented investigations are to understand the mechanisms of the mechanical behaviour of the spine structure and the role of its components, as well as the factors of its dysfunctions as scoliosis discopathy, spondylolisthesis. Also some mechanical effects of surgical interventions by total disc replacement is considered.

To account for the 3D character of the spine system including vertebrae, discs, ligaments, muscles etc. the finite element method (FEM) formulation was used throughout the paper. Some specific features of the structure are included in the models as non-conservative loads and muscular tension control performed by the nervous system. The finite element method together with CAD programs and experimental validation was used in investigations of a new type of artificial disc for lumbar spine. The stress analyses were performed for the prostheses being in clinical use and for some original new designs. The conclusions concern most important determinants of the mechanical behaviour of the system and the quality of the intervertebral disc prosthesis.

**Key words:** spine biomechanics, FEM, spinal disc prosthesis.

## 1. Introduction

A great majority of the scoliosis cases observed are idiopatics. There are various hypotheses concerning the ethiology of this disease available in the literature. It is usually assumed that scoliosis originates from a certain asymmetry revealed by a body or a kind of asymmetric functioning of the organism; e.g., asymmetric functioning of the muscular system. One can, however, accept the hypothesis that idiopatic scoliosis arises due to instability of the vertebral column system [1–4]. Even in case of a full symmetry there is always a possibility that primary curvature appears being an effect of buckling and paving the way to a full scoliosis. Elderly people after instability of their spinal column has emerged may suffer from pain due to the degeneration of intervertebral discs that follows.

It should be noted that experimental tests that can be made within biomechanics of human musculoskeletal system cover highly limited range [5]. Therefore, mathematical modelling of the human musculoskeletal system fosters the progress in this field, especially in view of the Finite Element Method (FEM) applications.

The finite element method is nowadays the most popular and commonly used tool for strain and stress analysis of engineering structures. The method has become widely known in biomechanics. FE computer programs and systems are of general nature and proved to be very useful in building even complex models of living tissues structures. FEM helps also to extract information concerning different aspects of vertebral column biomechanics [6–9]. In the FE models employed for investigations into deformations and stability of complex biological systems the following issues should be taken into account:

— The displacements of vertebral column elements reach the level on which the changes in vertebral column configuration should be included when deriving the equations of equilibrium;
— The internal forces affect substantially the stiffness of the whole system;
— The stiffness parameters; e.g. the Young modulus take much higher values in bones than the corresponding parameters of discs, muscles and ligaments;
— The intervertebral joints and rib cage joints impose constraints upon the relative motions of vertebrae and ribs;
— The pressures appearing in the system: in nucleus pulposa of intervertebral discs in abdominal cavity and in the rib cage are of non-conservative nature .

After satisfying all the requirements the aforementioned issues impose the final system of equations of equilibrium appears to be a non-linear one. The procedure of deriving these equations using FEM is given below [10].

*e-mail: mdietrich@ meil.pw.edu.pl

## 2. Non-linear equations of equilibrium for a system comprising both the rigid and elastic regions subject to conservative and non-conservative loads

Figure 1 shows a body described in the global Cartesian coordinate system $x$, that comprises the rigid region $V_s$ (representing the bone system) and the elastic region $V_e$ (representing soft tissues). The body is subject to the concentrated forces $\boldsymbol{Q}_1^e, \ldots \boldsymbol{Q}_i^e, \ldots \boldsymbol{Q}_n^e$, acting upon the elastic region and $\boldsymbol{Q}_1^s, \ldots \boldsymbol{Q}_i^s, \ldots \boldsymbol{Q}_n^s$ acting upon the rigid one, respectively.

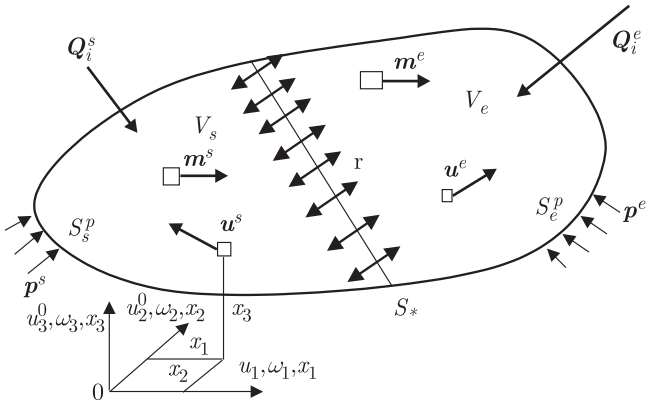


Fig. 1. Body comprising the rigid $V_s$ and elastic $V_e$ parts, respectively

The pressure $\boldsymbol{p}^e$ is acting upon the surface of elastic region $S_e^p$, while the surface of the rigid region $S_s^p$ is subject to the pressure $\boldsymbol{p}^s$. Additionally, the regions $V_e$ and $V_s$ are subject to the body forces consisting of the gravity and inertial forces, respectively, denoted as $\boldsymbol{m}^e$ and $\boldsymbol{m}^s$. The body was divided into 3D finite elements (sub-regions).

The displacements $\boldsymbol{u}^e$ appearing within the elastic region $V_e$ can be represented by the following equation [9]:

$$\boldsymbol{u}^e = \boldsymbol{N}\boldsymbol{q}_e, \tag{1}$$

where: $\boldsymbol{N}$ is the matrix of shape functions, determined for each finite element, while $\boldsymbol{q}_e$ represents the nodal displacements within the region $V_e$.

The displacements $\boldsymbol{u}^s$ appearing within the rigid region can be represented as follows:

$$\boldsymbol{u}^s = \boldsymbol{H}^0\boldsymbol{q}_s - \frac{1}{2}\boldsymbol{H}^1(\boldsymbol{q}_s)\boldsymbol{q}_s, \tag{2}$$

where:

$$\boldsymbol{H}^0 = \begin{bmatrix} 1 & 0 & 0 & 0 & x_3 & -x_2 \\ 0 & 1 & 0 & -x_3 & 0 & x_1 \\ 0 & 0 & 1 & x_2 & -x_1 & 0 \end{bmatrix}, \tag{3}$$

$$\boldsymbol{H}^1(\boldsymbol{q}_s) = \begin{bmatrix} \boldsymbol{q}_s^T\boldsymbol{R}^T & \begin{bmatrix} 0 & 0 & 0 \\ 0 & x_1 & 0 \\ 0 & 0 & x_1 \end{bmatrix} & \boldsymbol{R} \\ \boldsymbol{q}_s^T\boldsymbol{R}^T & \begin{bmatrix} x_2 & 0 & 0 \\ 0 & 0 & 0 \\ 0 & 0 & x_2 \end{bmatrix} & \boldsymbol{R} \\ \boldsymbol{q}_s^T\boldsymbol{R}^T & \begin{bmatrix} x_3 & 0 & 0 \\ 0 & x_3 & 0 \\ 0 & 0 & 0 \end{bmatrix} & \boldsymbol{R} \end{bmatrix}, \tag{4}$$

$$\boldsymbol{R} = \begin{bmatrix} 0 & 0 & 0 & 1 & 0 & 0 \\ 0 & 0 & 0 & 0 & 1 & 0 \\ 0 & 0 & 0 & 0 & 0 & 1 \end{bmatrix}, \tag{5}$$

$$\boldsymbol{q}_s^T = \begin{bmatrix} u_1^0 & u_2^0 & u_3^0 & \omega_1 & \omega_2 & \omega_3 \end{bmatrix}, \tag{6}$$

where: $u_1^0$, $u_2^0$, $u_3^0$ stand for the displacements along the axis $x$, while $\omega_1$, $\omega_2$, $\omega_3$ denote the angles of rotation. The displacements of points lying on the surface $S_*$, that separates the rigid region $V_s$ from the elastic one $V_e$, should have the same values in both the elastic and rigid regions. Upon the above condition one arrives at the following formula relating the vector $\boldsymbol{q}_s$ to $\boldsymbol{q}_e$

$$\boldsymbol{N}\boldsymbol{q}_e = \boldsymbol{H}^0\boldsymbol{q}_s - \frac{1}{2}\boldsymbol{H}^1(\boldsymbol{q}_s)\boldsymbol{q}_s\,, \quad (x_1, x_2, x_3) \in S_*\,, \tag{7}$$

Eq. (7) allows for determination of interactions between the elastic and rigid regions. These interactions, being in fact the surface loads, act upon the surface $S_*$ and in Fig. 1 are denoted as $\boldsymbol{r}$. Upon application of d'Alambert's principle the equations of equilibrium of the system can be written in the following form:

$$\begin{aligned} \boldsymbol{R}^Q = &\int_{V_e} \sigma_{ij}\delta e_{ij}dV - \int_{S_e^p} \boldsymbol{p}^e\delta\boldsymbol{u}^e dS - \sum_{i=1}^{m} \boldsymbol{Q}_i^e\delta\boldsymbol{u}_i^e \\ &- \int_{V_e} \boldsymbol{m}^e\delta\boldsymbol{u}^e dV - \int_{S_e^p} \boldsymbol{p}^s\delta\boldsymbol{u}^s dS - \sum_{i=1}^{n} \boldsymbol{Q}_i^s\delta\boldsymbol{u}_i^s \\ &- \int_{V_s} \boldsymbol{m}^s\delta\boldsymbol{u}^s dV - \int_{S^*} \boldsymbol{r}\left(\delta\boldsymbol{u}^s - \delta\boldsymbol{u}^e\right) dS = 0\,, \end{aligned} \tag{8}$$

where: $e_{ij}$ represents the strain tensor while $\sigma_{ij}$ stands for the stress tensor determined in the elastic region. After employing the matrix calculus procedures one can rewrite the strain tensor in the vector form follows:

$$\boldsymbol{\varepsilon} = \boldsymbol{D}^0\boldsymbol{u}^e + \frac{1}{2}\boldsymbol{D}^1\left(\boldsymbol{u}^e\right)\boldsymbol{u}^e\,, \tag{9}$$

$$\boldsymbol{\varepsilon} = \begin{bmatrix} e_{11} & e_{22} & e_{33} & 2e_{12} & 2e_{23} & 2e_{13} \end{bmatrix}^T, \tag{10}$$

where:

$$\boldsymbol{D}_0 = \begin{bmatrix} \frac{\partial}{\partial x_1} & 0 & 0 \\ 0 & \frac{\partial}{\partial x_2} & 0 \\ 0 & 0 & \frac{\partial}{\partial x_3} \\ \frac{\partial}{\partial x_2} & \frac{\partial}{\partial x_1} & 0 \\ 0 & \frac{\partial}{\partial x_3} & \frac{\partial}{\partial x_2} \\ \frac{\partial}{\partial x_3} & 0 & \frac{\partial}{\partial x_1} \end{bmatrix} \tag{11}$$

$$\boldsymbol{D}^1(\boldsymbol{u}^e) = \begin{bmatrix} \boldsymbol{u}^{eT}\partial_1^T\partial_1 \\ \boldsymbol{u}^{eT}\partial_2^T\partial_2 \\ \boldsymbol{u}^{eT}\partial_3^T\partial_3 \\ \boldsymbol{u}^{eT}\left(\partial_1^T\partial_2+\partial_2^T\partial_1\right) \\ \boldsymbol{u}^{eT}\left(\partial_2^T\partial_3+\partial_3^T\partial_2\right) \\ \boldsymbol{u}^{eT}\left(\partial_3^T\partial_1+\partial_1^T\partial_3\right) \end{bmatrix} \tag{12}$$

$$\partial_i = \begin{bmatrix} \frac{\partial}{\partial x_i} & 0 & 0 \\ 0 & \frac{\partial}{\partial x_i} & 0 \\ 0 & 0 & \frac{\partial}{\partial x_i} \end{bmatrix} \tag{13}$$

After substituting Eq. (1) into Eqs (9)–(13) the following formula for the strain tensor arises:

$$\boldsymbol{\varepsilon} = \boldsymbol{B}^0\boldsymbol{q}_e + \frac{1}{2}\boldsymbol{B}^1(\boldsymbol{q}_e)\boldsymbol{q}_e\,, \tag{14}$$

where:

$$\boldsymbol{B}^0 = \begin{bmatrix} \boldsymbol{N}_{1.,2} \\ \boldsymbol{N}_{2.,2} \\ \boldsymbol{N}_{3.,3} \\ \boldsymbol{N}_{2.,1}+\boldsymbol{N}_{1.,2} \\ \boldsymbol{N}_{2.,3}+\boldsymbol{N}_{3.,2} \\ \boldsymbol{N}_{1.,3}+\boldsymbol{N}_{3.,1} \end{bmatrix} \tag{15}$$

$$\boldsymbol{B}^1(\boldsymbol{q}_e) = \begin{bmatrix} \boldsymbol{q}_e^T\boldsymbol{N}_{,1}^T\boldsymbol{N}_{,1} \\ \boldsymbol{q}_e^T\boldsymbol{N}_{,2}^T\boldsymbol{N}_{,2} \\ \boldsymbol{q}_e^T\boldsymbol{N}_{,3}^T\boldsymbol{N}_{,3} \\ \boldsymbol{q}_e^T\left(\boldsymbol{N}_{,1}^T\boldsymbol{N}_{,2}+\boldsymbol{N}_{,2}^T\boldsymbol{N}_{,1}\right) \\ \boldsymbol{q}_e^T\left(\boldsymbol{N}_{,2}^T\boldsymbol{N}_{,3}+\boldsymbol{N}_{,3}^T\boldsymbol{N}_{,2}\right) \\ \boldsymbol{q}_e^T\left(\boldsymbol{N}_{,3}^T\boldsymbol{N}_{,1}+\boldsymbol{N}_{,1}^T\boldsymbol{N}_{,3}\right) \end{bmatrix} \tag{16}$$

$\boldsymbol{N}_{i.,j} = \frac{\partial}{\partial x_j}$ (the $i$-th row of matrix $\boldsymbol{N}$), $\boldsymbol{N}_{,j} = \frac{\partial}{\partial x_j}\boldsymbol{N}$.

On the assumption that the relationships between the strain and stress tensors are linear one can arrive at the formula for the stress tensor. Upon dividing the stress tensor into two parts: i.e., that due to the displacements and being an effect of muscle stimulation (the muscle modelling approach [10]) it can be written as:

$$\boldsymbol{\sigma} = \boldsymbol{\sigma}_1 + \boldsymbol{\sigma}_2\,, \tag{17}$$

where:

$$\boldsymbol{\sigma} = \begin{bmatrix} \sigma_{11} & \sigma_{22} & \sigma_{33} & \sigma_{12} & \sigma_{23} & \sigma_{13} \end{bmatrix}, \tag{18}$$

$$\boldsymbol{\sigma}_1^T = \boldsymbol{C}\boldsymbol{B}^0\boldsymbol{q}_e + \frac{1}{2}\boldsymbol{C}\boldsymbol{B}^1(\boldsymbol{q}_e)\boldsymbol{q}_e\,, \tag{19}$$

$$\boldsymbol{\sigma}_2^T = \boldsymbol{C}\boldsymbol{\lambda}\boldsymbol{p}\,. \tag{20}$$

$\boldsymbol{C}$ represents the matrix of anisotropic stiffness constants, $\boldsymbol{\lambda}$ stands for the matrix of contraction coefficients determined for each element separately and the vector $\boldsymbol{p}$ represents the stimulation magnitudes of all sub-regions of the region $V_e$. These stimulations affect in the element the deformations ($\boldsymbol{\lambda p}$) that develop in the direction determined by contraction coefficients (e.g. along the muscle fibres ) and generate stresses (11) in the element.

The pressures $\boldsymbol{p}^e$ and $\boldsymbol{p}^s$, acting over the surfaces $S_e^p$ and $S_s^p$, reveal a non-conservative nature. In the course of system deformation both the direction of elementary resultant force due to pressure and its magnitude change on the surface $S_e^p$.

Figure 2 shows the elementary area $S_e^p$ of the dimensions $dy_1$ and $dy_2$ before the body deformation. In the local coordinate system $y$ the axis $y_3$ coincides with the direction of pressure (at point $A$). This direction is determined by the normal $n$ to the surface $S_e^p$ passing through point $A$. Due to the body deformation the direction of normal $n$ changes (see line $n'$ in Fig. 2) and so does the elementary area. The latter can be approximately calculated from the formula $dy_1 \cdot dy_2(1+\varepsilon_1+\varepsilon_2)$, where $\varepsilon_1$ and $\varepsilon_2$ represent the strains along the axes $y_1$ and $y_2$, respectively. Assuming that the angles that make $n$ and $n'$ are

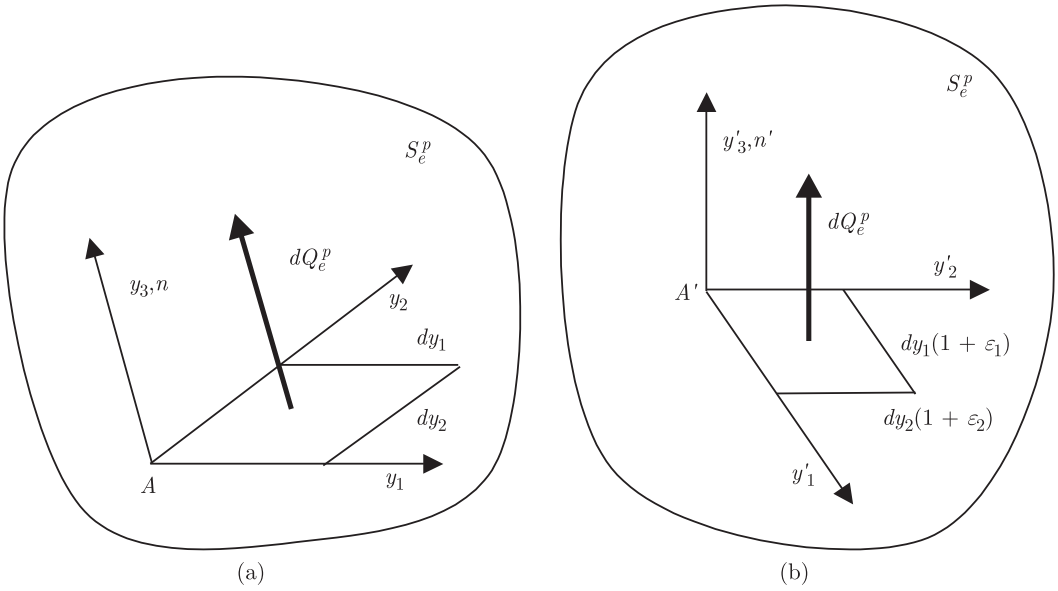


Fig. 2. The effect of $\boldsymbol{p}_e$ acting on the surface $S_e^p$ before (a) and after (b) the body deformation, respectively

small (neglecting the terms of higher order), the elementary resultant force $d\boldsymbol{Q}_e^p$ due to the pressure $\boldsymbol{p}^e$, relative to the fixed local coordinate system $y$ can be written as follows:

$$d\boldsymbol{Q}_e^p(\boldsymbol{q}_e) = |\boldsymbol{p}^e| dy_1 dy_2 \left[ -\frac{\partial v_3}{\partial y_1} \middle| -\frac{\partial v_3}{\partial y_2} \middle| 1 + \varepsilon_1 + \varepsilon_2 \right], \quad (21)$$

where: $\boldsymbol{v}$ represents the displacement vector relative to the fixed coordinate system $y$.

Let $\boldsymbol{A}$ denote the matrix of direction cosines of the angle the axes of global coordinate system $x$ make with the axes of local coordinate system $y$ then the derivative $\partial \boldsymbol{v}_i / \partial y_j$ can be determined in terms of $\partial u_i / \partial x_k$:

$$\frac{\partial \boldsymbol{v}_i}{\partial y_j} = \boldsymbol{A}_{kj} \boldsymbol{A}_{i1}^T \frac{\partial u_1}{\partial x_k}, \quad i,j,k = 1,2,3. \quad (22)$$

Substituting Eq. (1) into the above formula one can express the derivative $\partial \boldsymbol{v}_i / \partial y_j$ directly in terms of the vector of nodal displacements $\boldsymbol{q}_e$:

$$\frac{\partial v_i}{\partial y_j} = \boldsymbol{W}_{ij} \boldsymbol{q}_e \,, \quad (23)$$

where:

$$\boldsymbol{W}_{ij} = \boldsymbol{A}_{\cdot j}^T \left[ \begin{array}{c|c|c|c} \boldsymbol{A}_{\cdot i}^T & 0 & 0 & \boldsymbol{N}_{,1} \\ \hline 0 & \boldsymbol{A}_{\cdot i}^T & 0 & \boldsymbol{N}_{,2} \\ \hline 0 & 0 & \boldsymbol{A}_{\cdot i}^T & \boldsymbol{N}_{,3} \end{array} \right], \quad (24)$$

while $\boldsymbol{A}_{\cdot k}$ stands for the $k$-th column of matrix $\boldsymbol{A}$. Substituting $\boldsymbol{v}$ for the vector $\boldsymbol{u}^e$ into Eq. (9) and using Eq. (23), the formula for $\varepsilon_1 + \varepsilon_2$ appears as follows:

$$\varepsilon_1 + \varepsilon_2 = \boldsymbol{G}^0 \boldsymbol{q}_e + \frac{1}{2} \boldsymbol{G}^1(\boldsymbol{q}_e) \boldsymbol{q}_e \,, \quad (25)$$

where:

$$\boldsymbol{G}^0 = \boldsymbol{W}_{11} + \boldsymbol{W}_{22} \,, \quad (26)$$

$$\boldsymbol{G}^1(\boldsymbol{q}_e) = \boldsymbol{q}_e^T \left( \boldsymbol{W}_1^T \boldsymbol{W}_1 + \boldsymbol{W}_2^T \boldsymbol{W}_2 \right) \,, \quad (27)$$

$$\boldsymbol{W}_i^T = \left[ \boldsymbol{W}_{1i}^T \middle| \boldsymbol{W}_{2i}^T \middle| \boldsymbol{W}_{3i}^T \right]. \quad (28)$$

Upon substituting Eqs (23) and (25) into Eq. (21), the elementary force $d\boldsymbol{Q}_e^p$ can be represented in the global coordinate system $x$ as follows:

$$d\boldsymbol{Q}_e^p(\boldsymbol{q}_e) = |\boldsymbol{p}_e| dy_1 dy_2 \left[ 0 \middle| 0 \middle| 1 \right] \boldsymbol{A}^T + |\boldsymbol{p}_e| dy_1 dy_2 . \cdot \boldsymbol{q}_e^T \left[ -\boldsymbol{W}_{31}^T \middle| -\boldsymbol{W}_{32}^T \middle| \boldsymbol{G}^{0T} + \tfrac{1}{2} \boldsymbol{Q}^{1T}(\boldsymbol{q}_e) \right] \boldsymbol{A}^T . \quad (29)$$

Following the same procedure one can determine the formula for the elementary resultant force $d\boldsymbol{Q}_e^p$ due to the pressure $\boldsymbol{p}^s$ acting on the surface $S_s^p$, in the fixed local coordinate system $y$:

$$d\boldsymbol{Q}_s^p = |\boldsymbol{p}^s| dy_1 dy_2 \left[ \Theta_2 \middle| -\Theta_1 \middle| 1 \right] \quad (30)$$

where: $\Theta_1$ and $\Theta_2$ represent the angles of rigid body rotation about the axes $y_1$ and $y_2$. The angle of rotation $\Theta_1$ and $\Theta_2$ can be determined in terms of the angles of rotation $\omega_1,\ \omega_2,\ \omega_3$ representing the rigid body rotation in the global coordinate system $x$:

$$\Theta_1 = \boldsymbol{A}_{\cdot 1}^T \, \boldsymbol{R} \, \boldsymbol{q}_s \,, \quad (31)$$

$$\Theta_2 = \boldsymbol{A}_{\cdot 2}^T \, \boldsymbol{R} \, \boldsymbol{q}_s \,, \quad (32)$$

where the matrix $\boldsymbol{R}$ and the vector $\boldsymbol{q}_s$ are represented by Eqs (5) and (6), respectively. Substituting Eqs (31) and (32) into Eq. (30), one obtains the formula for the elementary force $d\boldsymbol{Q}_s^p$ in the global coordinate system, as follows:

$$d\boldsymbol{Q}_s^p = |\boldsymbol{q}^s| dy_1 dy_2 \left[ 0 \middle| 0 \middle| 1 \right] \boldsymbol{A}^T + + |\boldsymbol{p}^s| dy_1 dy_2 \boldsymbol{q}_s^T \left[ \boldsymbol{R}^T \boldsymbol{A}_{\cdot 1} \middle| -\boldsymbol{R}^T \boldsymbol{A}_{\cdot 2} \middle| 0 \right] \boldsymbol{A}^T . \quad (33)$$

The following formula for virtual deformations can be obtained after employing Eq. (14):

$$\delta \boldsymbol{\varepsilon} = \boldsymbol{B}^0 \delta \boldsymbol{q}_e + \frac{1}{2} \boldsymbol{B}^1(\boldsymbol{q}_e) \delta \boldsymbol{q}_e + \frac{1}{2} \delta \boldsymbol{B}^1(\boldsymbol{q}_e) \boldsymbol{q}_e \,. \quad (34)$$

Since the matrix $\boldsymbol{B}^1$ is linear with respect to $\boldsymbol{a}$ and $\boldsymbol{b}$, i.e. $\boldsymbol{B}^1(\boldsymbol{a})\boldsymbol{b} = \boldsymbol{B}^1(\boldsymbol{b})\boldsymbol{a}$ we arrive at the following formula for the virtual deformations:

$$\delta \boldsymbol{\varepsilon} = \boldsymbol{B}^0 \delta \boldsymbol{q}_e + \boldsymbol{B}^1(\boldsymbol{q}_e) \delta \boldsymbol{q}_e \,. \quad (35)$$

Upon application of Eq. (1) the virtual displacements in the elastic region $V_e$ can be written in the following way:

$$\delta \boldsymbol{u}^e = \boldsymbol{N} \delta \boldsymbol{q}_e \,. \quad (36)$$

The following formula for virtual displacements within the rigid region $V_s$ may be obtained from Eq. (2) taking into consideration the fact that the matrix $\boldsymbol{H}^1(\boldsymbol{q}_s)$ is linear also with respect to arbitrary vectors $\boldsymbol{a}$ and $\boldsymbol{b}$:

$$\delta \boldsymbol{u}^s = \boldsymbol{H}^0 \delta \boldsymbol{q}_s - \boldsymbol{H}^1(\boldsymbol{q}_s) \delta \boldsymbol{q}_s \,. \quad (37)$$

To simplify the calculations it occurs very convenient to represent the mass loads $\boldsymbol{m}^e$ and $\boldsymbol{m}^s$ in terms of the mass loads $\boldsymbol{m}_\gamma^e$ and $\boldsymbol{m}_\gamma^s$ due to gravity forces and the inertial loads $\boldsymbol{m}_a^e$ and $\boldsymbol{m}_a^s$ due to accelerations. The load vectors $\boldsymbol{m}_\gamma^e$ and $\boldsymbol{m}_\gamma^e$ can be written as follows:

$$\boldsymbol{m}_\gamma^e = \left[ \gamma_{x1}^e \middle| \gamma_{x2}^e \middle| \gamma_{x3}^e \right], \quad (38)$$

$$\boldsymbol{m}_\gamma^s = \left[ \gamma_{x1}^s \middle| \gamma_{x2}^s \middle| \gamma_{x3}^s \right], \quad (39)$$

where: $\gamma_{xi}^e,\ \gamma_{xi}^s$ stand for the mass forces due to the gravity acting in the direction coincident with those of the corresponding axes of global coordinate system $x$.

One can arrive at the formulae for the body accelerations in the elastic $V_e$ and rigid $V_s$ regions, respectively after differentiating twice Eqs (1) and (2) with respect to time:

$$\ddot{\boldsymbol{u}}^e = \boldsymbol{N} \ddot{\boldsymbol{q}}_e \,, \quad (40)$$

$$\ddot{\boldsymbol{u}}^s = \boldsymbol{H}^0 \ddot{\boldsymbol{q}}_s - \boldsymbol{H}^1(\boldsymbol{q}_s) \ddot{\boldsymbol{q}}_s - \boldsymbol{H}^1(\dot{\boldsymbol{q}}_s) \dot{\boldsymbol{q}}_s \,. \quad (41)$$

Let $\rho_e$ and $\rho_s$ stand for the mass densities in the regions $V_e$ and $V_s$, respectively, then the formulae for $\boldsymbol{m}_a^e$ and $\boldsymbol{m}_a^e$ can be rewritten as follows:

$$\boldsymbol{m}_a^e = -\rho_e \ddot{\boldsymbol{q}}_e^T \boldsymbol{N}^T \,, \quad (42)$$

$$\boldsymbol{m}_a^e = -\rho \ddot{\boldsymbol{q}}_s^T \left( \boldsymbol{H}^{0T} - \boldsymbol{H}^{1T}(\boldsymbol{q}_s) \right) + \rho_s \dot{\boldsymbol{q}}_s^T \boldsymbol{H}^{1T}(\dot{\boldsymbol{q}}_s) \,. \quad (43)$$

Upon substituting Eqs (17)–(43) into Eq. (8) and after necessary transformations one can arrive at the following form of

equations of equilibrium for the elastic region of the body:

$$\boldsymbol{R}_e(\boldsymbol{q}_e) = \boldsymbol{R}_e^0 + \int\limits_{V_e} \boldsymbol{B}^{0T}\boldsymbol{\sigma}_1^T dV + \int\limits_{V_e} \boldsymbol{B}^{1T}(\boldsymbol{q}_e)\boldsymbol{\sigma}^T dV - \int\limits_{S_e^p} |\boldsymbol{p}^e| \boldsymbol{N}^T \boldsymbol{A} \begin{bmatrix} -\boldsymbol{W}_{31} \\ -\boldsymbol{W}_{32} \\ \boldsymbol{G}^0 + \frac{1}{2}\boldsymbol{G}^1(\boldsymbol{q}_e) \end{bmatrix} \boldsymbol{q}_e dS = 0\,, \tag{44}$$

where:

$$\boldsymbol{R}_e^0 = \int\limits_{V_e} \boldsymbol{B}^{0T}\boldsymbol{\sigma}_2^T dV - \int\limits_{S_e^p} |\boldsymbol{p}_e| \boldsymbol{N}^T \boldsymbol{A} \begin{bmatrix} 0 \\ 0 \\ 1 \end{bmatrix} dS - \sum_{i=1}^{m} \boldsymbol{N}_i^T \boldsymbol{Q}_i^{eT} - \int\limits_{V_e} \boldsymbol{N}^T \boldsymbol{m}_\gamma^{eT} dV + \int\limits_{V_e} \rho_e \boldsymbol{N}^T \boldsymbol{N} \ddot{\boldsymbol{q}}_e dV - \int\limits_{S_*} \boldsymbol{N}^T \boldsymbol{r}^T dS \tag{45}$$

and for the rigid one:

$$\begin{aligned} \boldsymbol{R}_s(\boldsymbol{q}_s) = \boldsymbol{R}_s^0 &+ \int\limits_{S_s^p} |\boldsymbol{p}^s| \boldsymbol{H}^{1T}(\boldsymbol{q}_s) \boldsymbol{A} \begin{bmatrix} 0 \\ 0 \\ 1 \end{bmatrix} dS \\ &- \int\limits_{S_s^p} |\boldsymbol{p}^s| \boldsymbol{H}^{0T} \boldsymbol{A} \begin{bmatrix} \boldsymbol{A}_{\cdot 1}^T \boldsymbol{R} \\ -\boldsymbol{A}_{\cdot 2}^T \boldsymbol{R} \\ 0 \end{bmatrix} dS \\ &+ \int\limits_{S_s^p} |\boldsymbol{p}^s| \boldsymbol{H}^{1T}(\boldsymbol{q}_s) \boldsymbol{A} \begin{bmatrix} \boldsymbol{A}_{\cdot 1}^T \boldsymbol{R} \\ -\boldsymbol{A}_{\cdot 2}^T \boldsymbol{R} \\ 0 \end{bmatrix} \boldsymbol{q}_s dS \\ &+ \sum_{i=1}^{n} \boldsymbol{H}_i^{1T}(\boldsymbol{q}_s) \boldsymbol{Q}_i^{sT} \\ &+ \int\limits_{V_s} \boldsymbol{H}^{1T}(\boldsymbol{q}_s) \boldsymbol{m}_\gamma^{sT} dV \\ &- \int\limits_{V_s} \rho_s \boldsymbol{H}^{0T} \boldsymbol{H}^1(\boldsymbol{q}_s) \ddot{\boldsymbol{q}}_s dS \\ &- \int\limits_{V_s} \rho_s \boldsymbol{H}^{1T}(\boldsymbol{q}_s) \boldsymbol{H}^0 \ddot{\boldsymbol{q}}_s dV \\ &+ \int\limits_{V_s} \rho_s \boldsymbol{H}^{1T}(\boldsymbol{q}_s) \boldsymbol{H}^1(\boldsymbol{q}_s) \ddot{\boldsymbol{q}}_s dV \\ &+ \int\limits_{V_s} \rho_s \boldsymbol{H}^{1T}(\boldsymbol{q}_s) \boldsymbol{H}^1(\boldsymbol{q}_s) \boldsymbol{q}_s dV \\ &- \int\limits_{S_*} \boldsymbol{H}^{1T}(\boldsymbol{q}_s) \boldsymbol{r}^T dS = 0\,, \end{aligned} \tag{46}$$

where:

$$\boldsymbol{R}_s^0 = -\int\limits_{S_s^p} |\boldsymbol{p}^s| \boldsymbol{H}^{0T} \boldsymbol{A} \begin{bmatrix} 0 \\ 0 \\ 1 \end{bmatrix} dS - \sum_{i=1}^{n} \boldsymbol{H}_i^{0T} \boldsymbol{Q}_i^{sT} - \int\limits_{V_s} \boldsymbol{H}^{0T} \boldsymbol{m}_\gamma^{sT} dV + \int\limits_{V_s} \rho_s \boldsymbol{H}^{0T} \boldsymbol{H}^0 \ddot{\boldsymbol{q}}_s dV - \int\limits_{V_s} \rho_s \boldsymbol{H}^{0T} \boldsymbol{H}^1(\dot{\boldsymbol{q}}_s) \dot{\boldsymbol{q}}_s dV + \int\limits_{S_*} \boldsymbol{H}^{0T} \boldsymbol{r}^T dS\,. \tag{47}$$

The systems of ordinary differential equations represented by Eqs (44) and (46) should be complemented by the consistency equations of displacements on the surface $S_*$, represented by Eq. (7). These are non-linear differential equations representing the body motion. In the case when external forces and tensions arising in the muscular system change in a quasi-static way one can neglect the terms representing in Eqs (44) and (45) the inertial forces, so that we arrive at algebraic non-linear equations. In the example shown below these equations have been solved using the Newton-Raphson method.

## 3. Deformations of the vertebral column under symmetric loading

After solving Eqs (44) and (46) we obtain the deformations (displacements) of vertebral column points the magnitude of critical buckling load and the form of equilibrium corresponding to it.

The FE model of human vertebral column applied to the aforementioned analyses was presented in detail by the Authors elsewhere [2, 6, 10].

The results presented below were obtained from the analysis of a full symmetry of the loads acting upon the system. It was assumed that the human vertebral column in straight position is subject to the load due to the trunk weight estimated as 300 N as well as due to the forces corresponding to the weights held in both hands. These forces changed within the range from 0 N to 698 N. The vertebral column configuration was analysed under growing external loads in terms of observing its deformation forms (modes). It was also assumed that tensions in muscular system counterbalanced the external forces to keep the body in straight position, and the muscle actions comply with the energy criterion [12, 13].

When following the solving procedure of the set of equations Eq. (44)–(46) the external load action was simulated in several steps of small increments. Relatively small increments were employed for the load magnitude at which the configuration of equilibrium changed qualitatively, i.e. from symmetrical to the asymmetrical one.

Figure 3 shows the vertebral column deformations and vertical displacements in the saggital plane under the load due to the trunk weight (Fig. 3a) and additionally due to the weight held in hands equal to $2 \times 191.5$ N = 383 N (Fig. 3b). Sample tensions in the fibres of back erector for the aforementioned loads are shown in Fig. 6a and Fig. 6b. It is clearly seen that the vertebral column deformations and tensions in muscles are symmetrical with respect to the saggital plane. Due to the load

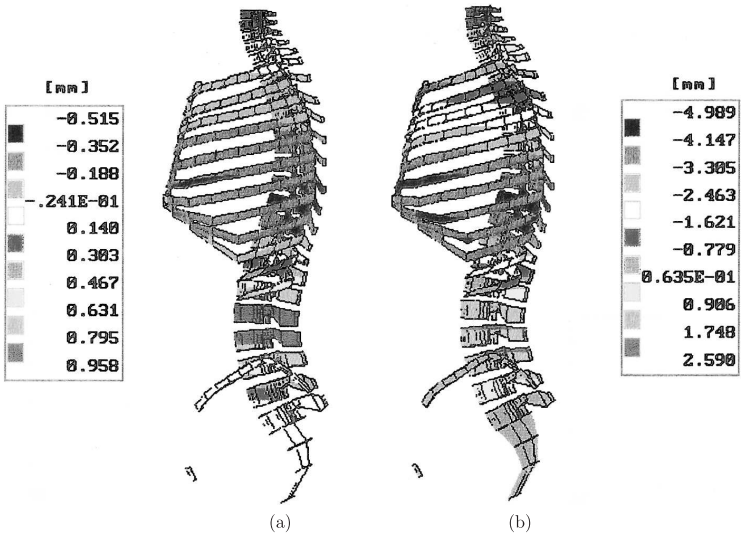


Fig. 3. Vertical displacements of the vertebral column in the saggital plane, representing stable symmetrical form of equilibrium, appearing due to: a) body weight equal to 300 N; b) body weight and the weight held in both hand equal to $2 \times 191,5$ N = 383 N

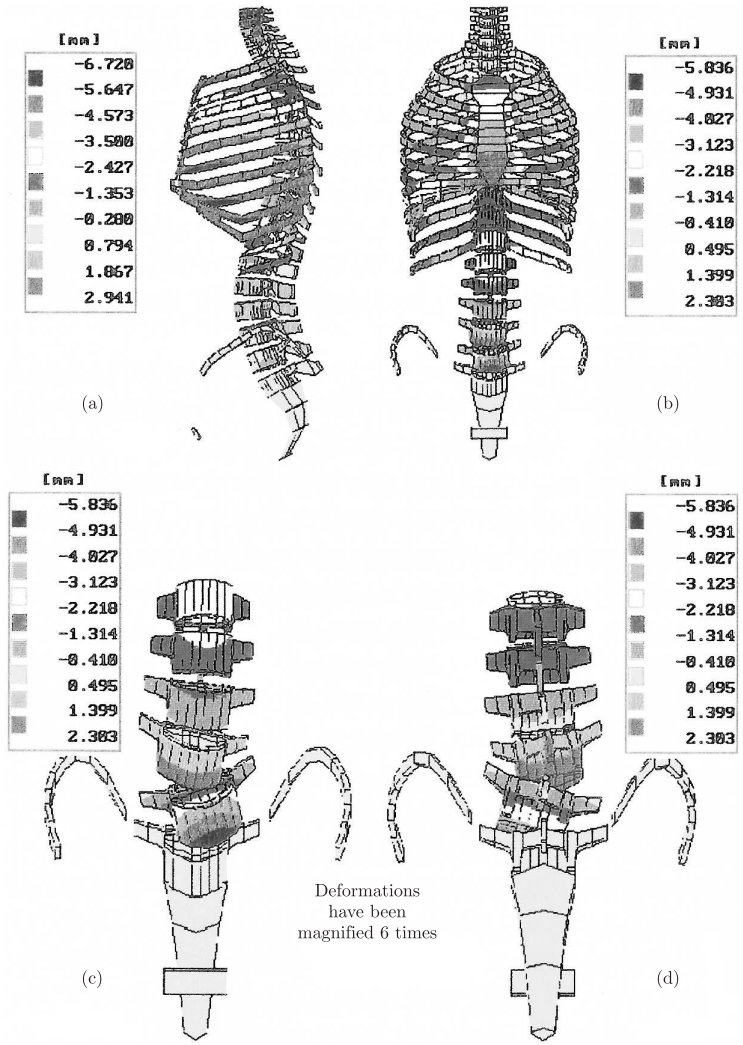


Fig. 4. Vertical displacements of the vertebral column representing the stable asymmetrical form of equilibrium due to the body weight equal to 300 N and the weights held in both hands equal to $2 \times 211.5$ N = 423 N a) in the saggital plane; b) and c) in the frontal plane – front view; d) in the frontal plane – rear view

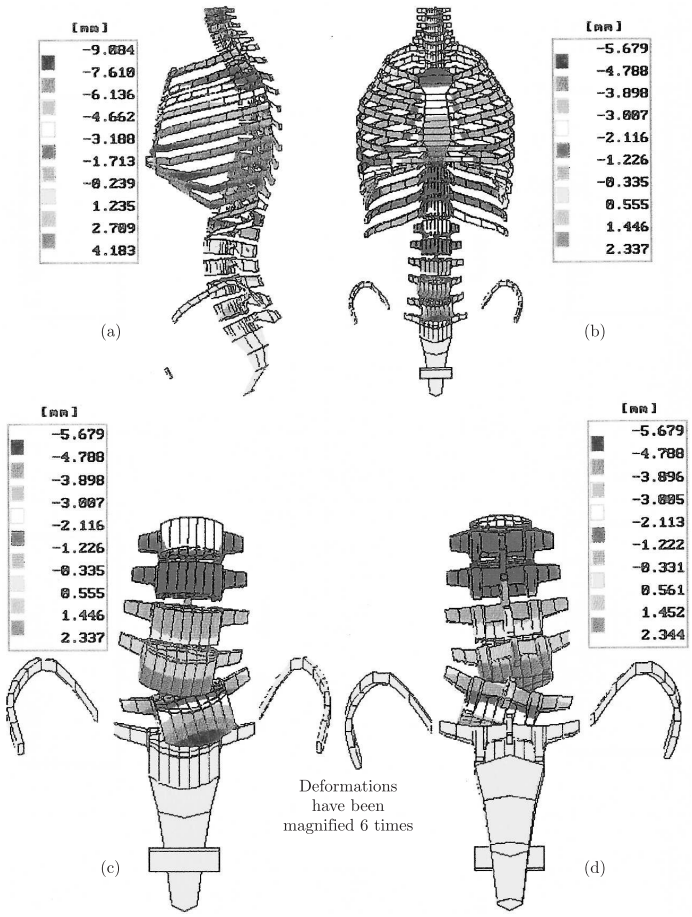


Fig. 5. Vertical displacements of the vertebral column representing the stable asymmetrical form of equilibrium due to the body weight equal to 300 N and the weights held in both hands equal to $2 \times 311.5$ N = 623 N a) in the saggital plane; b) and c) in the frontal plane – front view; d) in the frontal plane – rear view

actions the natural curvatures of vertebral column, i.e. lordosis and kyphosis, increase.

Upon increasing the weights held in hands up to $2 \times 211.5$ N = 423 N the asymmetrical form of equilibrium shown in Fig. 4 results from solving Eqs (44)–(46). The form of vertebral column equilibrium has changed since the symmetrical configuration was not stable and therefore could not ensure the equilibrium between the external forces and those arising in the muscular system. The asymmetrical form of equilibrium reveals higher lordosis and kyphosis and rotations of lower lumbar vertebrae (Fig. 4c,d). Those vertebra displacements and rotations can be considered as a small primary curvature that develops then into scoliosis. The tensions in the back erector extensor shown in Fig. 6c also reveal asymmetry with respect to the saggital plane. No further qualitative changes in the form of equilibrium appear as the external load grows. One can observe only an increase in displacements and rotations of vertebrae (see Fig. 5) as well as higher tensions in muscles (see Fig. 6d). The deformation form differs more significantly from the symmetrical one shown in Fig. 3. The vertebral column looses its stability when the weights held in hands reach the magnitude of $2 \times 349$ N = 698 N. Both the symmetrical and asymmetrical configurations become unstable. The tensions in the muscular system are no longer capable of balancing the external loads. It means, in fact that the man should throw the weights to protects the vertebral column (ligaments, muscles, discs, etc) from damages.

## 4. Artificial vertebral lumbar disc

Permanent exceeding of critical loads causing large deformations along the lumbar segment may involve, especially in elderly people, damages and degeneration of intervetebral discs that manifest through a back pain. About 80% people experience back pain at least once in their lifetime and for many of them spinal disorders and especially the low back disorders are a real problem. The lower part of spine; i.e., consists of 5 vertebrae, named L1 to L5, connected by the intervertebral discs. The lumbar segment links the upper body with the pelvis and exerts a great influence on the mobility and strength of human body. The vertebral column is a very complex structure which consists of vertebrae, intervertebral discs, ligaments, muscles and spinal cord (Fig. 7). The vertebral bone is mainly the orthotropic trabecular bone tissue surrounded by the cortical shell [14].

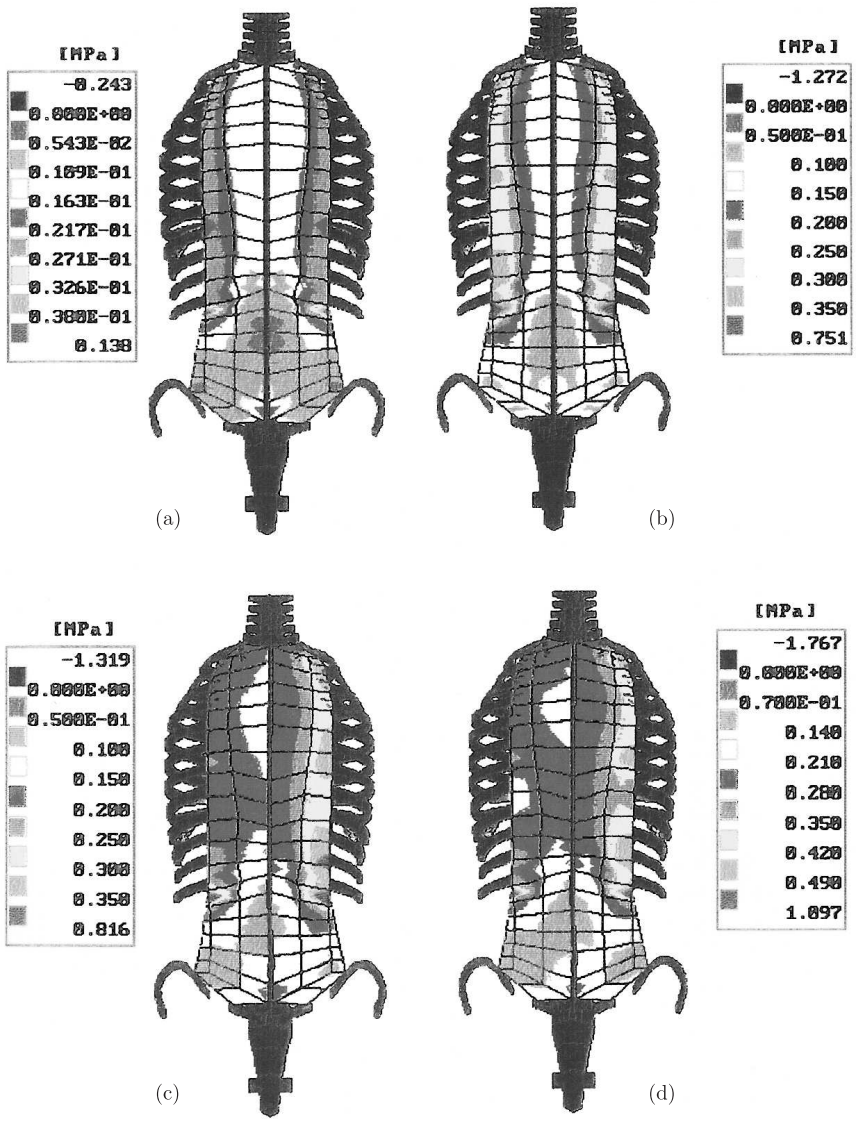


Fig. 6. Tensions in fibres of the back erector (rear view) due to: a) body weight equal to 300 N (symmetrical form of equilibrium); b) body weight and the weights held in both hands equal to $2 \times 191.5$ N = 383 N (symmetrical form of equilibrium), c) body weight and the weights held in both hands equal to $2 \times 211.5$ N = 423 N (asymmetrical form of equilibrium); d) body weight and the weights held in both hands equal to $2 \times 311.5$ N = 623 N (asymmetrical form of equilibrium)

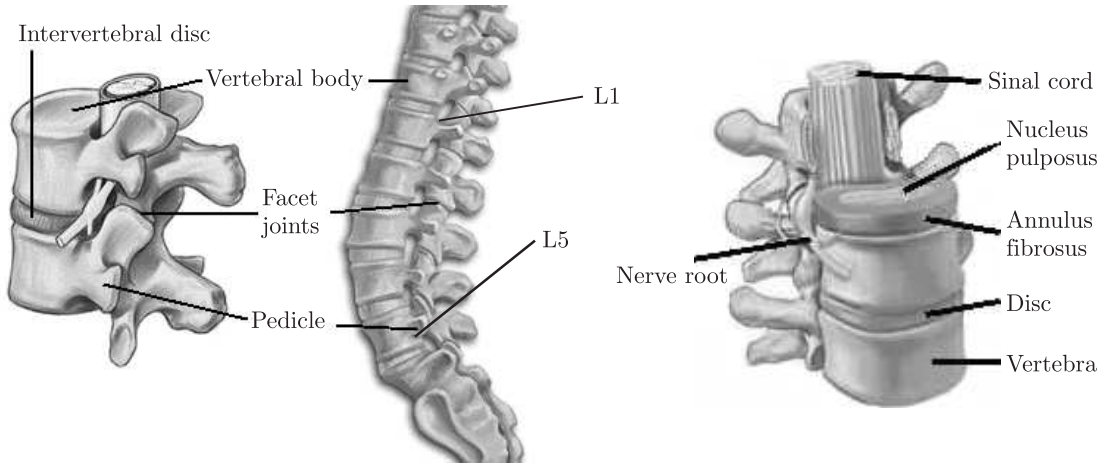


Fig. 7. Anatomy of the lumbar spine

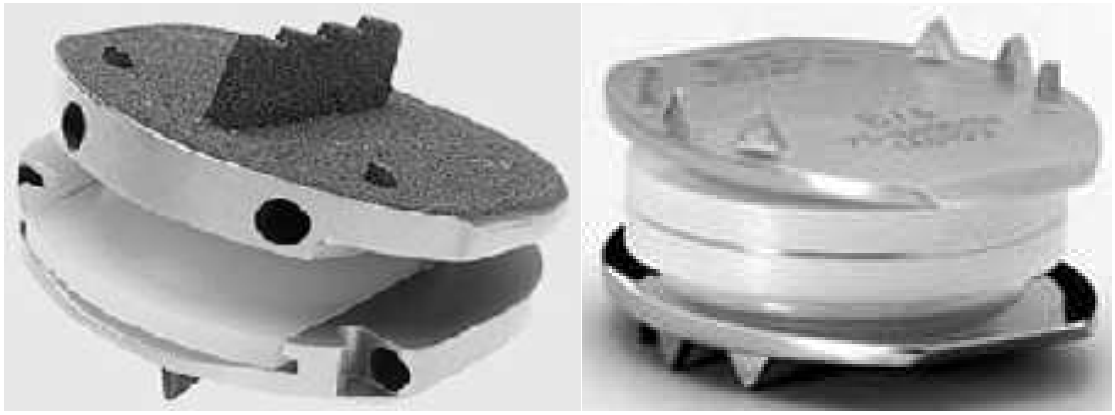

(a) (b)

Fig. 8. Total disc prostheses: a) ProDisc (Waldemar Link) and b) Charite III (Aesculap)

Each disc is composed of the following three different tissues:

— Annulus – a strong fibrous ligament surrounding the disc;
— Nucleus – a liquid middle, surrounded by the annulus. The internal hydrostatic pressure within the nucleus helps in proper transfer of compression loads;
— Endplates – cartilage structures which attach the disc to the vertebral bodies.

Non-surgical treatment for people with neck and back pain caused by disc disorders includes rest, heat, pain medications, chiropractic manipulation and physical therapy. Unfortunately, these treatments fail in a significant number of patients. In the cases when such a treatment fails, surgery is the next possible solution. This usually means spinal fusion surgery. Unfortunately, there are a number of drawbacks to undergoing a spinal fusion. The vertebral bodies often do not fuse well and the fusion itself increases stiffness and decreases spine mobility. As a result the stresses increase above and below, respectively, of the modified segment. This may cause new problems but in another parts of the vertebral column. Since the 1960s, when artificial hips and knees were introduced in clinical practice, many surgeons have believed that the artificial disc may improve the results of surgical treatment for many types of back pain [15,16].

One of the major advantages the artificial disc reveals consists in preserving mobility of the adjacent vertebrae. There are in general the following two types of artificial discs in practical use: nuclear prosthesis – designed to replace only the soft inner core of a disc and total disc prosthesis – designed to replace a full disc (annulus, nucleus and endplates). The advantage of replacing the entire disc is that the patient may avoid time-degeneration of the annulus. Artificial discs have been in clinical use in Europe for more than 10 years. Most popular are the SB Charite from Waldemar Link Company and the ProDisc manufactured by Aesculap. In the USA the total disc arthroplasty is still considered to be an experimental technique. Both, the ProDisc and Charite prostheses (Fig. 8), consist of two metal endplates and the middle made of polyethylene. They reveal a little different mobility in frontal and saggital planes, respectively.

The rotation about the vertical axis is free and limited only by the surrounding structures i.e. ligaments and muscles. The stability is ensured in the case of Charite prosthesis by the teeth-like spikes and in the case of ProDisc by the spikes and the large keel.

There are other devices currently in development, some of them patented [16], including those used for replacing of the nucleus as well as the facet joints. Theoretical and experimental investigations are currently conducted to make a progress in the field [17].

The best way to estimate quality of a new design is to perform the finite element stress and strain analysis for the model of structure consisting of the spine segment and prosthesis. The quality of the implant behaviour depends strongly on the strength of endoprosthesis and its fixation [18]. The failure reasons of the biomechanical implant-living tissues systems are rather complex and are believed to be connected with non-uniform stress distribution within the bone-implant system. Numerical simulation techniques of bone-implant systems mechanical behaviour can reduce the number of animal experiments and clinical investigations in the process of new implants design. As compared to experimental techniques they offer great advantages. They enable the same bone model to be used for different devices and allow for analysis of the influence of different device parameters on load transfer and stress distribution [19]. In experimental models the adequate representation of biological tissues may be, for many reasons, difficult.

## 5. Mechanical factors determining the quality of total disc replacement

It is usually assumed that the artificial disc replacement aims at replication of the normal motion of the disc in the vertebral column. There are various factors the designers must keep in mind as they develop an artificial disc [20]. The device should maintain a proper intervertebral spacing, allow for a full range of motion keeping the same axes of rotations and provide the

required stability. It has to be made up of parts securely attached to each other in order to facilitate insertion during the surgical procedure and minimize the possibility of spinal cord injury. The prosthesis must act as a shock absorber and should be very durable. Because the average age of a patient undergoing the disc replacement is about 40 years the strength of the prosthesis must be perfect to avoid the necessity for revision surgery. It must be made of materials that are safe to be implanted in the human body and do not cause allergic reactions. The interaction between the implant and the living tissues should not cause also high stress concentrations in other parts of the spine. It would be helpful for the surgeons if the artificial disc were made of a material that visible in an X-ray picture or using other imaging techniques.

In the presented study it has been assumed that the disc prosthesis should work in the same way and undergo similar mechanical conditions as the natural disc in the healthy spine. Some of the figures presenting these conditions, taken from the literature are presented in Fig. 9.

## 6. FE modelling of the interaction between the total disc prosthesis and the vertebral column segment

The natural intervertebral disc and different designs of the disc prosthesis were examined by performing the stress and strain analysis using FEM and ANSYS system. Developing of the accurate FE model is usually a laborious and time-consuming task. This may be overcome in terms of parametric FE modelling, recently often used – with different approaches to the problem, by engineers [11,21,22].

In a parametric model many different possible shapes should be taken into account with a limited number of parameters. After a modification of the parameters representing e.g. geometrical and material properties of the considered object one can obtain a new model in a relatively short time. Despite many advantages, the parametric model reveals also some drawbacks. The process of producing such a FE model is more difficult than in the case of the non-parametric one. Therefore it is reasonable to do this only in the case when the model is to be used many times. In this study an attempt was made at creating of the FE model of a lumbar vertebral column segment and then more detailed model of two vertebrae motion segment with an artificial disc. Both the vertebrae and the intervertebral disc are represented in a parametrical way. Such a model may be helpful in the cases when we deal with the problem of new design or with a prosthesis of the custom-made type.

In the model the co-ordinates of characteristic points are assumed to be parameters representing the shape of the bones. A special attention was focused on the accurate representation of a vertebral body. The coordinates of 70 points in 3D space have been used in the description of its shape. A relatively high number of the points allows for accurate representation of curvatures of upper and bottom vertebrae surfaces, which is important since those surfaces may contact with an artificial intervertebral disk. The shapes of other vertebral parts were described in a simplified way.

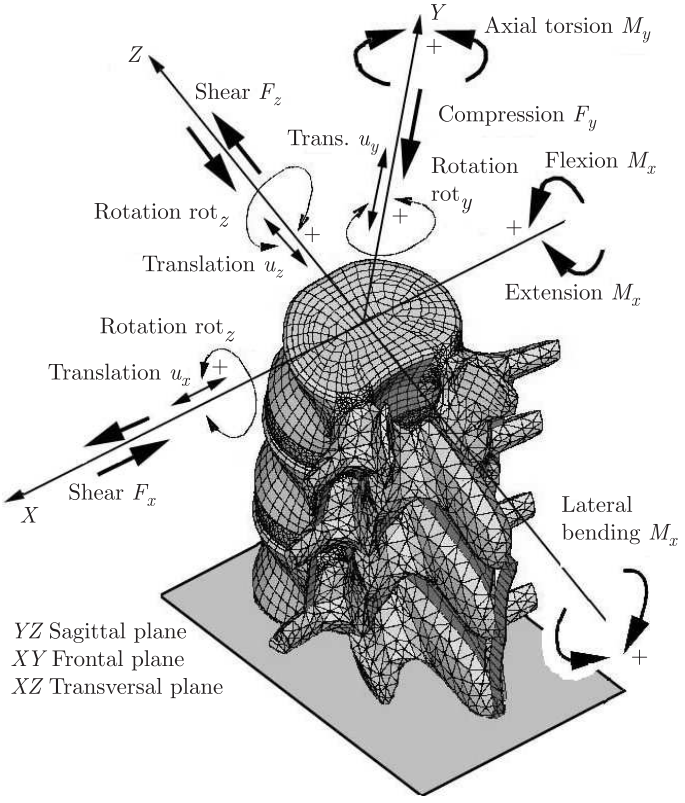


| Loads considered, mobility | |
|---|---|
| Compression | $F_y = 3000$ N |
| Shear | $F_z = 300$ N |
| Shear | $F_x = 300$ N |
| Extension/Flexion rot$_x$ range: –5°,+10° | $M_x = 12$ Nm |
| Lateral bending rot$_z$ range: –7.5°,+7,5° | $M_z = 8$ Nm |
| Axial torsion rot$_y$ range: –2°,+2° | $M_y = 3.1$ Nm |

Fig. 9. Some of the parameters specifying mechanical requirements for the total disc prosthesis

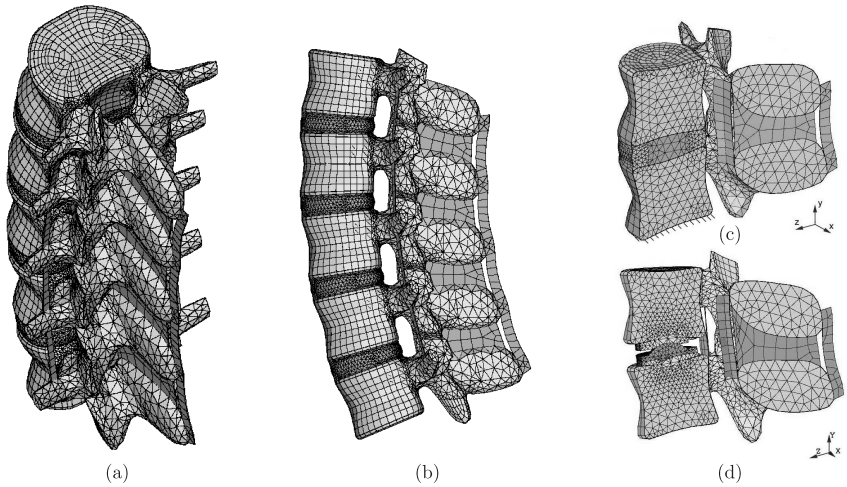


Fig. 10. Finite element model of a vertebral column segment: a) FE mesh, general view, b) cross-section in the sagittal plane, c) cross-section of the motion segment with natural disc, d) cross-section of the motion segment with artificial disc

The points were used to generate 3D spline curves over which the surfaces defining the solids were spanned. Those solids were divided into 3D solid finite elements, which represent the region of the spongy bone. The external vertebral surfaces were divided into shell finite elements, which represent the cortical bone. The shell thickness of particular shell elements corresponding to the cortical shell may differ depending on the position and serve also as parameters of the numerical model. The division into the finite elements is performed automatically with a mesh density required by the user. In a similar way the FE model of an artificial disk is built. An example of such a FE model is presented in Fig. 10. The standard material properties used in numerical analyses are presented in the Table 1. In some cases orthotropic mechanical properties of the bone tissues were taken into account. Since the process of modelling with such assumptions accepted is complicated and a slight influence on the obtained results is exerted the isotropic models of cortical and trabecular tissues were used as the standard in comparative analyses.

Table 1
Material properties used in the comparative analyses

| Material | Young modulus E (MPa) | Thickness $\delta$ (mm) | Poisson's ratio $v$ |
|---|---|---|---|
| Cortical shell | 12000 | 1.5 | 0.3 |
| Cancellous core | 100 | – | 0.4 |
| Nucleus | 0.012 | – | 0.499 |
| Annulus | 10 | – | 0.35 |
| Ligaments | 10 | 2 | 0.3 |
| Polyethylene | 1200 | – | 0.35 |
| Co-Cr Alloy | 210000 | – | 0.3 |

The main goal of the analyses was to estimate stresses within the bones and the implant. The design of the intervertebral disc should ensure a relatively uniform stress distribution within the bone tissue to enable the proper bone reconstruction processes. The stresses within the implant parts have to remain below the assumed limits.

## 7. Finite element analyses of the prostheses in clinical use

First analyses were carried out for the ProDisc and Charite III prostheses. Their FE models are presented in Fig. 11 and Fig. 12, respectively.

At the first stage the prostheses were investigated with the surrounding structures of spinal segment. Then the loads and boundary conditions were applied using simplified model of the prosthesis and the two adjacent vertebrae. The contact with polyethylene friction ($\mu = 0.05$) was assumed between

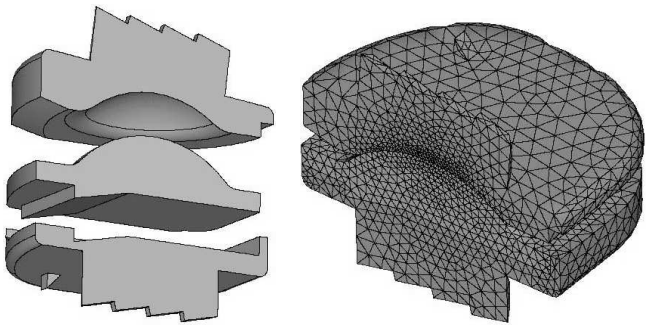

Fig. 11. FE model of ProDisc prosthesis

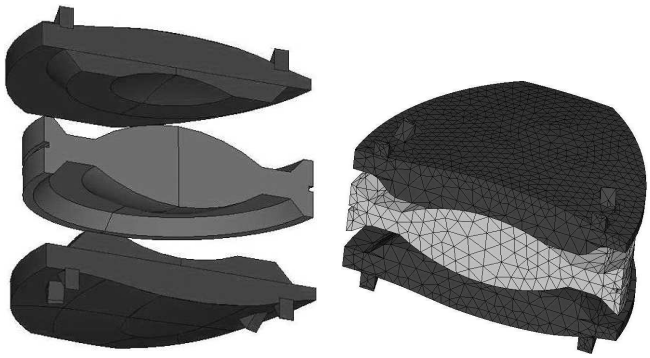

Fig. 12. FE model of Charite III artificial disc

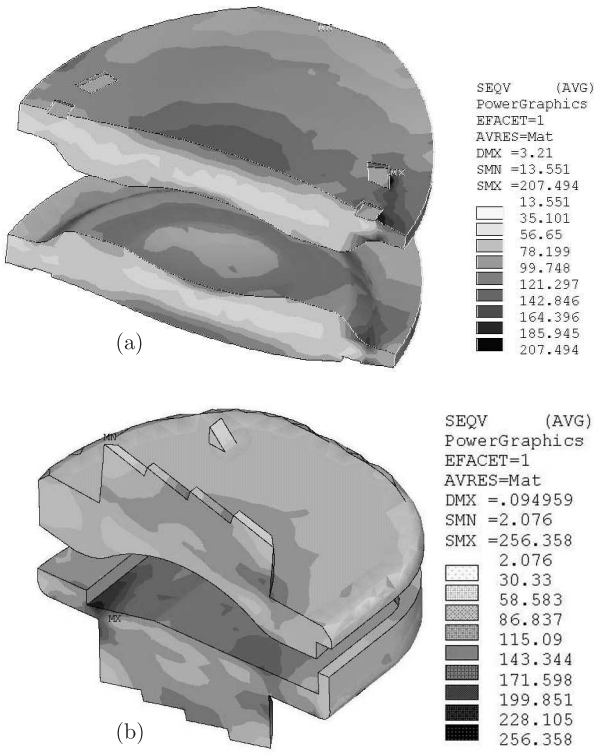


Fig. 13. Von Mises equivalent stresses (MPa) in metal plates of prostheses: a) ProDisc; b) Charite III

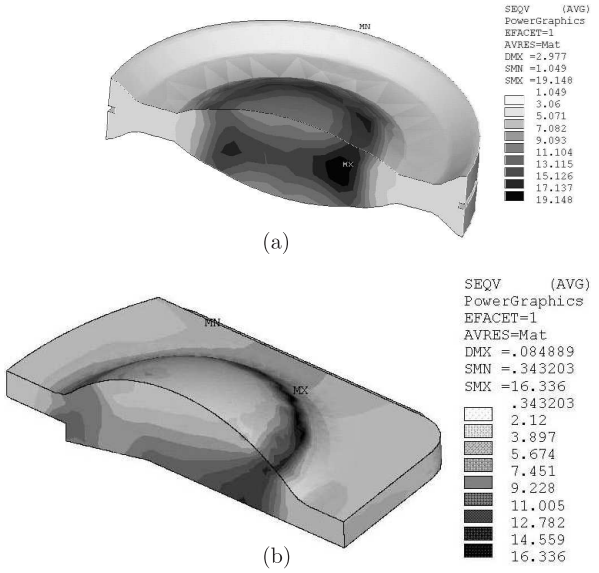


Fig. 14. Von Mises equivalent stresses (MPa) in the polyethylene inlays of prostheses: a) ProDisc; b) Charite III

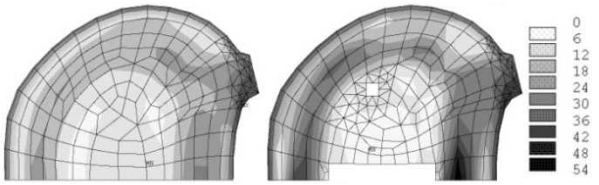


Fig. 15. Von Mises equivalent stress distribution (MPa) on the top surface of lower vertebra for the compression 3000N

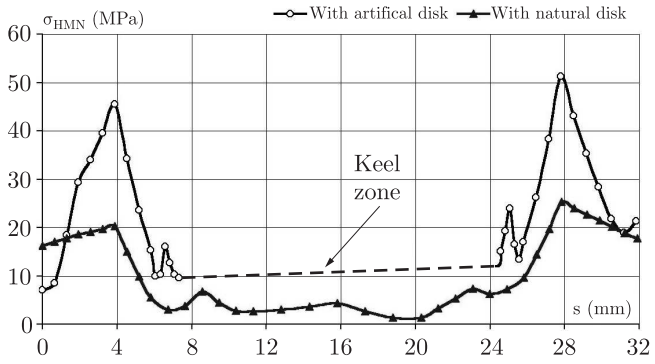


Fig. 16. Von Mises equivalent stress distribution (MPa) on the top surface of the lower vertebra along the path at the symmetry plane YZ (see Fig. 15)

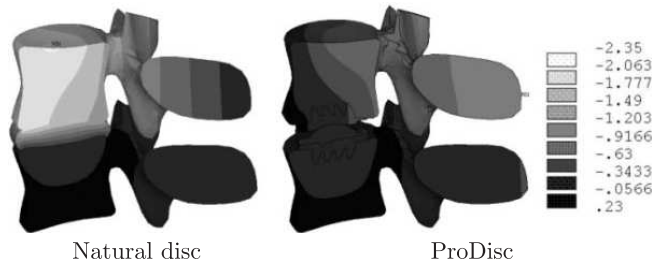


Fig. 17. Vertical displacement (mm) distribution due to the 3000 N compression

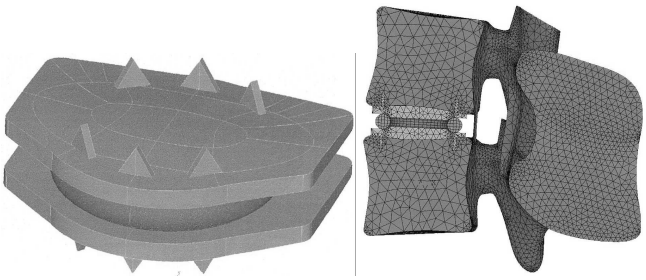

Fig. 18. The artificial disc with toroidal middle

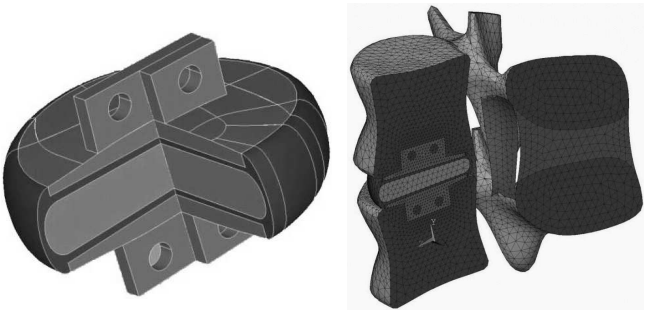

Fig. 19. The artificial disc with the inlay being thick walled container filled with the gel

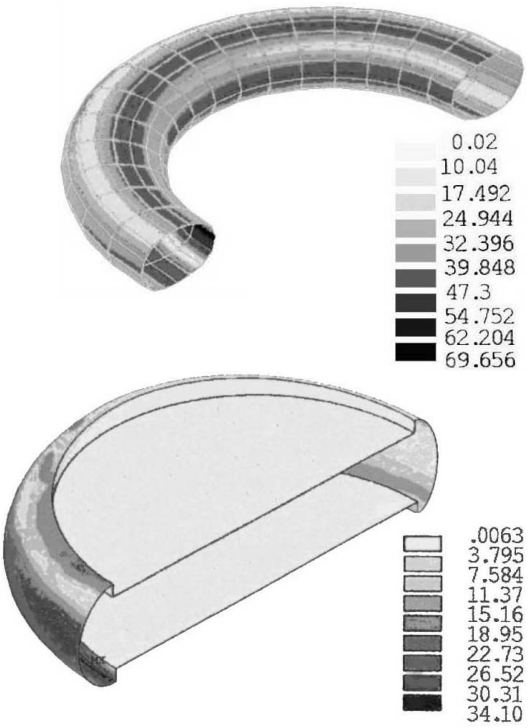


Fig. 20. Von Mises equivalent stresses (MPa) in polyethylene elements of the new designs (the results correspond to compression analysed for the models showed in Figs 18 and 19)

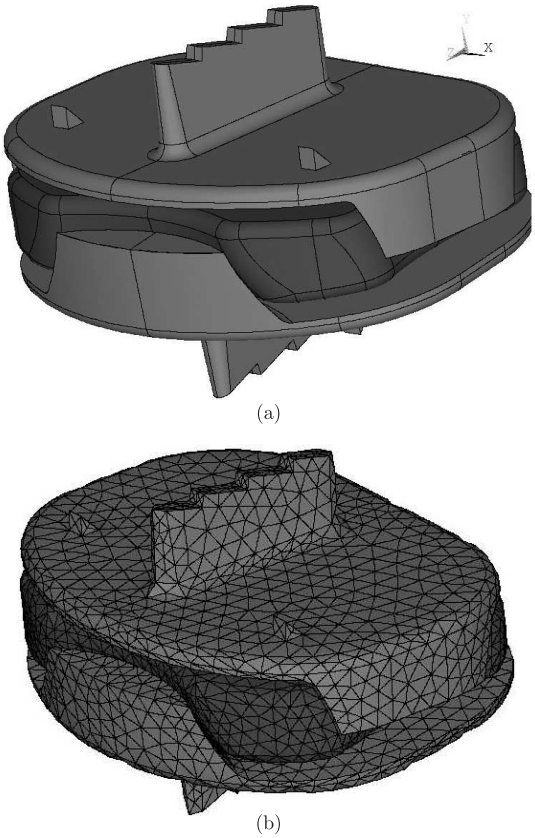


Fig. 21. FE model of the considered new prosthesis: geometrical model (a) and its discretisation (b)

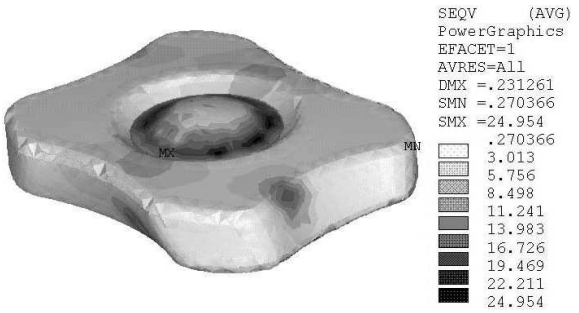


Fig. 22. Von Mises equivalent stresses in the polyethylene part of the new prosthesis (compression)

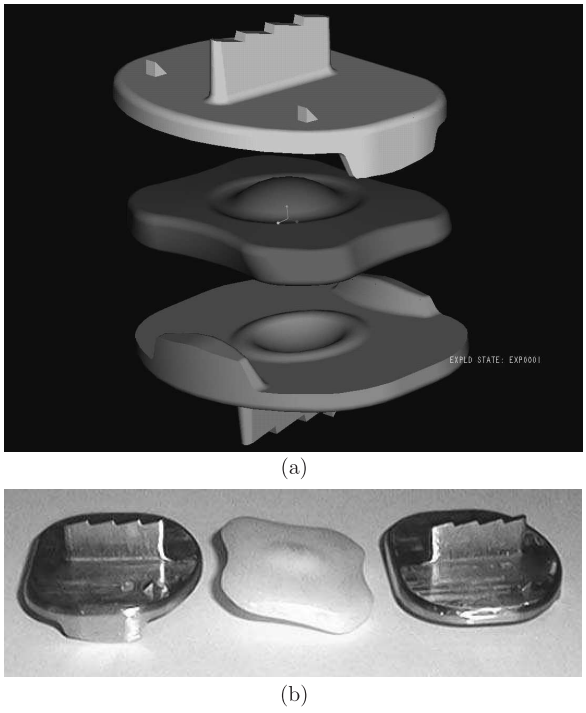


Fig. 23. The CAD model of the new design (a) and the prototype (b)

the metal plates and the inlay in the case of Charite III prosthesis. In the case of ProDisc prosthesis the contact elements were used between upper metal plate and polyethylene inlay but lower metal plate and inlay were glued. The Von Mises equivalent stresses within the metal plates for the compressive force $F_y = 3000$ N are presented in Fig. 13. The results for the inlays are presented in Fig. 14.

The similar maximum von Mises stresses were obtained for the prostheses (about 200 MPa in metal parts and about 20 MPa in the inlay). It should be mentioned that metal plates material on the exterior side was extended and on the interior one was compressed as a result of bending. The highest stress concentrations appeared in the keel-plate and teeth-plate transition regions and were caused by rapid stiffness changes and the notch effect. Nearly the hydrostatic compression state was observed for the spherical parts of polyethylene inlay.

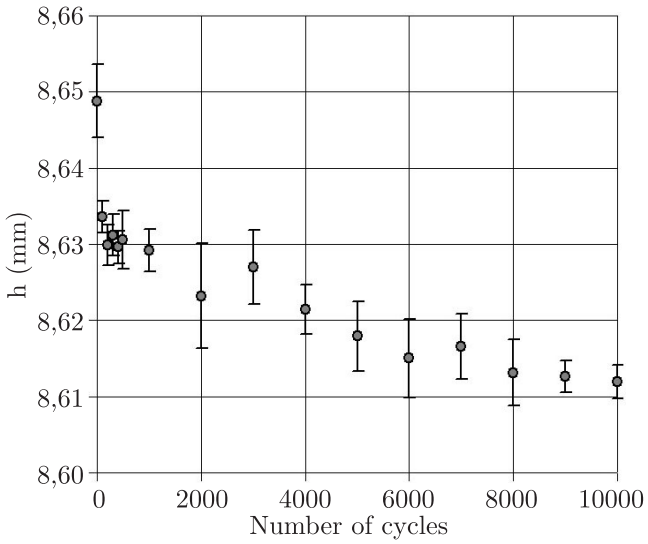


Fig. 24. The experimental stand for strength, fatigue and wear tests (a) and the resulting height of the artificial disc as the function of assumed load cycles

The important information concerning the quality of the new design may be obtained from comparing the behaviour of the analysed system with a natural disc and with the artificial one. In the presented example the artificial disc causes higher stresses within the bone (Figs 15, 16) but the stress distribution is similar to that corresponding to the natural case. The greater differences are observed when comparing the vertical displacements what result from stiffness differences between both the considered cases (Fig. 17).

## 8. New solutions and FEA results

The different ideas and solutions to the problem were examined. At the beginning new designs shown in Fig. 18 and Fig. 19 were taken into consideration. The first one consisted of metal plates with a toroidal middle; the second one was built of metal plates and a soft polyethylene cushion with hydrogel inside it. The hyperelastic Money-Rivlin material model was used for the hydrogel. In both the FE models the contact with friction was assumed between different parts of the structures and the hydrogel was modelled as a material bonded to the polyethylene shell.

Unfortunately these solutions (Figs 18, 19) failed due to too high stresses arising in the cushion (Fig. 20).

The artificial disc presented in Fig. 21 was designed in order to carry shear forces and to allow for a certain range of axial rotation. The design comprises two concave endplates of cobalt-chromium-molybdenum alloy and the elastic inlay. The plates have the large keel and the two teeth that grip into the vertebral body above and below the disc. A specially shaped polyethylene middle is placed between the two endplates (Fig. 21 and Fig. 22). The mobility of the structure fulfils the assumed requirements: extension-flexion within the range (–5°, 10°), lateral bending (–7.5°, 7.5°) and axial torsion (–4.5°, 4.5°) respectively.

In the examined case (compression and axial rotation) boundary conditions were the same as those in the ProDisc investigation. The torsional moment $M_y = 3.1$ Nm and compressive force $F_y = 3000$ N were applied. Contact elements were placed between adjacent metal and polyethylene surfaces (friction ($\mu = 0.05$). The maximum stresses in the polyethylene inlay were similar to those appearing in the ProDisc and stress concentrations appeared in the same places (Fig. 22). The analysis of the design show the relatively uniform stress distribution within the metal parts and in surrounding bone tissues. Different modifications of this design are investigated.

To verify the results of FE analysis and to provide the supplementary information about mechanical behavior of the prosthesis some experimental investigations are being performed using the prototype of the design (Fig. 23).

The prototype of the prosthesis is tested during mechanical experiments. The stand (Fig. 24), fully controlled by the computer, is equipped with two stepping motors which allow imitating flexion, compression and axial rotation. It is possible to conduct the investigations either with a dry prosthesis or with a prosthesis immersed into physiological fluid. The performed experiments include measurements of the relative displacements within the structure and strain gauges analysis of stresses within the prosthesis parts. The stand enables also wear and fatigue investigations.

## 9. Conclusions

The magnitudes of critical loads for the vertebral column resulting from calculations allow one to make certain generalisa-

tions about the ethiology of some types of scoliosis. The magnitude of critical load at which an abnormal deformation of the vertebral column arises combined with displacements and rotations of vertebrae depends on a variety of its parameters, e.g., stiffness, assumed configuration of equilibrium, the kind of external loads and the way of their action, etc. Total stiffness of the vertebral column appears as a sum of elastic (passive) stiffness and a geometrical (caused by internal stresses) one. The elastic stiffness of the system is generated mainly by the stiffness of such elements like: discs, ligaments, cartilages and muscles. The so-called geometrical stiffness results from the conjugation between the stresses and non-linear terms of geometrical relations (9) and depends on the magnitudes, direction and distributions of the internal forces emerging in the system; i.e., stresses in discs and ligaments, forces acting upon rigid elements, tensions in muscles, etc. It may increase or decrease the total stiffness of the system changing that way the magnitude of critical load.

The criteria of muscular system control that have been applied take into account only a static work done by the human. Upon application of the criteria of minimisation of forces in muscles or those used in the present paper, that minimise the elastic energy, the external load is balanced mainly by tensions in muscles of large cross-sections and producing large moments like the back erector. The tensions in short muscles of small cross-sections and producing large moments reveal relatively low magnitudes. They are, however, also necessary for the sake of system stability, playing the role of elements that stabilise the vertebral column. One can, therefore, assume that the primary cause of scoliosis consists in improper way of muscular tension control performed by the human nervous system (not necessarily involving asymmetry of tensions in muscles). Such a situation may arise due to e.g. abnormalities of the nervous system, hypoplasia of muscles – especially the short ones or improper habits acquired by the patient during his lifetime.

The improper (in the stability aspect) tension in muscles may cause the appearance of initially very small (even maybe unnoticeable) asymmetrical form of equilibrium even under a very low external load, especially in children whose muscular and skeletal systems develop. Further consequences consist in continuous rebuilding of the skeletal system causing durable deformation of the vertebral column.

Suitable corrective exercises strengthening the muscular system (especially the short muscles) may prevent from appearance and development of scoliosis in terms of increasing the magnitude of critical load.

One can also consider the efficiency of the surgical method used in treatment of scoliosis, e.g., the Harrington method, which, roughly speaking consists in restoring to a possible extent, the proper shape of the vertebral column, using bars and abduction splints. That way one can affect, after a while, the repeated (and this time tending properly) rebuilding of the skeletal system. This method, however, removes only the consequences of the initiated scoliosis. If no changes are introduced into the muscle control or the way of proper muscle development is not ensured (which is extremely difficult due to the bars and abduction splints introduced) the process of scoliosis will re-initiate. The research of intervertebral lumbar prosthesis shows that numerical simulation appears to be a very important pre-clinical test of a new design of an intervertebral disc. The FE modelling enables to estimate the stresses in living structures and within the investigated prostheses. The first designs appeared to be unsatisfactory because of too high stresses in the prosthesis components. However the design showed in Fig. 21 presents similar mechanical behaviour as the prostheses in clinical use.

Hydrostatic compression in the polyethylene inlay is an advantageous feature because it reduces the equivalent stresses within it. The analyses showed that the important factor of prosthesis quality is the proper fitting of endplates to vertebral body surfaces. For that reason the shape of the endplates will be improved in the next modification of the design. In the future step also the size of the keel should be reduced in order to improve the stress distribution and allow for a less invasive implantation technique.

## REFERENCES


[1] A. Bergmark, *Mechanical Stability of the Human Lumbar Spine*, Lund Instytute of Technology, Department of Solid Mechanics, 1987.

[2] M. Dietrich, K. Kędzior, K. Miller, and T. Zagrajek, "Statics and stability of human spine under working conditions". W.S. Marras et al. (eds.), *The Ergonomics of Manual Work*, pp. 147–150, Taylor and Francis, London – Washington D.C., 1993.

[3] M. Dietrich, K. Kędzior, A. Wittek, and T. Zagrajek, "Nonlinear finite element analysis of formation and treatment of intervertebral disc hermiae", *Proc. Institution of Mech. Engrs.* part H, 206, 225–234 (1992).

[4] P.J. Weiler, G.M. McNeice, and B.J. Medley, "An experimental study of the buckling behaviour of 1-rod implants used in the surgical treatment of scoliosis", *Spine* 11 (2), 992–998 (1986).

[5] M. Dietrich (ed.), "Medical biomechanics of spine-theory, modelling and clinical applications", *Lecture Notes of the Intern. Centre of Biocybernetics Seminars* 20, (1993).

[6] M. Dietrich, K. Kędzior, and T. Zagrajek, "A biomechanical model of the human spinal system", *Proc. Instn. Mech. Engrs.* Part H, 205, 19–26 (1991).

[7] K. Kędzior, G. Krzesiński, and T. Zagrajek, "Numerical simulation of the scoliosis as caused by mechanical response of the spinal segment to external load", *Lecture Notes of the Intern. Centre of Biocybernetics Seminars* 33, 158–164 (1996).

[8] W. Skalli, "Spine biomechanics. From basic research to clinical applications", *Acta of Bioengineering and Biomechanics* 1, Suppl. 1, 379–384 (1999).

[9] O.C. Zienkiewicz and R.L. Taylor, *The Finite Element Method*, McGraw-Hill, London, 1991.

[10] T. Zagrajek, *Biomechanic Modelling of Spinal System by Finite Element Method*, Office House PW, Warsaw, 1990.

[11] C.M. Whyne, S. Hu, and C. Lotz, "Parametric finite element analysis of vertebral bodies affected by tumors", *Journal of Biomechanics* 34, 1317–1324 (2001).

[12] M. Dietrich, K. Kędzior, and T. Zagrajek, "Modelling of muscle action and stability of the human spine", J. Winters, S.L.-Y. Woo (eds): *Multiple Muscle Systems – Biomechanics and Movement Organization*, New York, Springer-Verlag, 451–460 (1990).

[13] K. Kędzior and T. Zagrajek, "A biomechanical model of the human musculoskeletal system", A. Morecki and K. Waldron (eds.): *Human and Walking Machine Locomotion*, pp. 125–152, Springer-Verlag, Wien, 1997.

[14] A.A. White and M.M. Panjabi, *Clinical Biomechanics of the Spine*, J.B. Lippincott Company, 1990.

[15] J.P. Lemaire, W. Skalli, F. Lavaste, A. Templier, F. Mendes, A. Diop, V. Sauty, and E. Lalouz, "Intervertebral disc prosthesis, results and prospectus for the year 2000", *Clin. Orthop.* 337, 64–76 (1997).

[16] M. Szpalski, R. Gunzburg, and M. Mayer, "Spine arthoplasty: a historical review", *European Spine Journal* 1 (Suppl. 2), 65–84 (2002).

[17] C. Pezowicz, "Analysis of phenomena occuring in the intervertebral disc under different load conditions", *Acta of Bioengineering and Biomechanics* 5, (Suppl. 1), 379–384 (2003).

[18] G. Krzesiński, "Numerical methods in analysis and design of implants", *Lecture Notes of the Intern. Centre of Biocybern.: Biomechanics. Customized Endoprostheses*, 48–58 (2003).

[19] M. Dietrich, K. Kędzior, G. Krzesiński, and T. Zagrajek, "Selected problems of orthopaedic implants design – numerical approach", *Proceedings of Tenth World Congress on the Theory of Machines and Mechanisms*, 1799–1804, Oulu (1999).

[20] R. Bertagnoli, and S. Kumar, "Indications for full prosthetic disc arthoplasty: a correlation of clinical outcome against a variety of indications", *European Spine Journal* 11 (Suppl. 2), 131–136 (2002).

[21] M. Dietrich, K. Kędzior, G. Krzesiński, T. Zagrajek, and B. Zielińska, "Parametric finite element models of human bones", *Acta of Bioengineering and Biomechanics* 4, 135–136 (2002).

[22] M. Dietrich, K. Kędzior, K. Skalski, T. Zagrajek, G. Krzesiński, J. Skoworodko, P. Borkowski, and P. Wymysłowski, "On concurrent engineering and design of an intervertebral disc of lumbar spine", *18-th Conference on Computer-aided Production Engineering CAPE*, Professional Engineering Publishing Limited, UK, 209–219 (2003).